Chemical exchange at the tri-nuclear copper centre of small laccase from Streptomyces coelicolor

Dasgupta R., Sai Sankar Gupta K.B., Nami F., Groot H.J.M. de, Canters G.W., Groenen E.J.J., Ubbink M.

Biophysical *Journal*
Biophysical Letter

Biophysical Society

Chemical Exchange at the Trinuclear Copper Center of Small Laccase from *Streptomyces coelicolor*

Rubin Dasgupta,[1] Karthick B. S. S. Gupta,[2] Faezeh Nami,[1,2] Huub J. M. de Groot,[1] Gerard W. Canters,[2] Edgar J. J. Groenen,[2] and Marcellus Ubbink[1,*]
[1]Gorlaeus Laboratories, Leiden Institute of Chemistry, Leiden University, Leiden, The Netherlands and [2]Huygens-Kammerlingh Onnes Laboratory, Leiden Institute of Physics, Leiden, The Netherlands

ABSTRACT The trinuclear copper center (TNC) of laccase reduces oxygen to water with very little overpotential. The arrangement of the coppers and ligands in the TNC is known to be from many crystal structures, yet information about possible dynamics of the ligands is absent. Here, we report dynamics at the TNC of small laccase from *Streptomyces coelicolor* using paramagnetic NMR and electron paramagnetic resonance spectroscopy. Fermi contact-shifted resonances tentatively assigned to histidine Hδ1 display a two-state chemical exchange with exchange rates in the order of 100 s^{-1}. In the electron paramagnetic resonance spectra, at least two forms are observed with different g_z-values. It is proposed that the exchange processes reflect the rotational motion of histidine imidazole rings that coordinate the coppers in the TNC.

SIGNIFICANCE To our knowledge, this is the first report that shows chemical exchange in the trinuclear copper center of a laccase that is attributed to the motion of the coordinating histidine rings. The potential catalytic relevance of this motion leads toward a better understanding of oxygen reduction by small laccase, inspiring the design of efficient enzymatic biofuel cells.

Laccases reduce dioxygen to two water molecules at the trinuclear copper center (TNC) by oxidizing a broad range of substrates at the type 1 (T1) site, with very little overpotential (1), making them potentially interesting proteins for enzymatic biofuel cells. The TNC (Fig. 1 *d*) comprises a type 3 (T3) site with two coppers and a type 2 (T2) site with a single copper. The T1 site is linked to the TNC via a conserved HCH motif, and the two are separated by ~13 Å. This conserved motif provides a fast route for electron transfer from the substrate via the T1 site to the TNC for O_2 reduction to water. Crystal structures of laccases (2–8) have helped in modeling the catalytic mechanism of O_2 reduction (2,4). The current model for the catalytic mechanism for O_2 reduction at the TNC is summarized in Scheme S1. In brief, the resting oxidized (RO) state is converted to fully reduced (FR) state by receiving four electrons from substrate oxidized at the T1 site. The FR state can bind oxygen and is converted to peroxide intermediate state by transferring two electrons to the oxygen molecule, hence forming a peroxide. The peroxide intermediate state is converted to native intermediate (NI) state, in which the oxygen bond has been cleaved, and all the coppers in the TNC are coupled via an oxygen atom. This NI state can slowly be converted to RO state in the absence of the substrate or directly go into the FR state in the presence of the substrate (2–4). Although much is known about the mechanism through different models, mimicking the active site to design artificial catalyst is notoriously difficult. The model compounds reported so far do not have the catalytic efficiency of the enzyme (9–12). Usually, dynamics associated with the residues at the active site is ignored while designing artificial catalyst, although it was reported that motions can be important for electron and proton transfer processes (13–16). Determining such motions in laccase might provide insight into designing a functional framework for an efficient artificial catalyst. Here, we report the presence of conformational exchange at the TNC on the millisecond timescale, ascribed to motions of the copper-coordinating imidazole rings of histidine residues.

For this study, a mutant of small laccase from *Streptomyces coelicolor* (SLAC) was used, in which the T1 site is copper depleted by the C288S mutation (SLAC-T1D) (8). Machczynski et al. showed that the wild-type (wt)

Submitted March 11, 2020, and accepted for publication May 11, 2020.
*Correspondence: m.ubbink@chem.leidenuniv.nl
Editor: Wendy Shaw.
https://doi.org/10.1016/j.bpj.2020.05.022

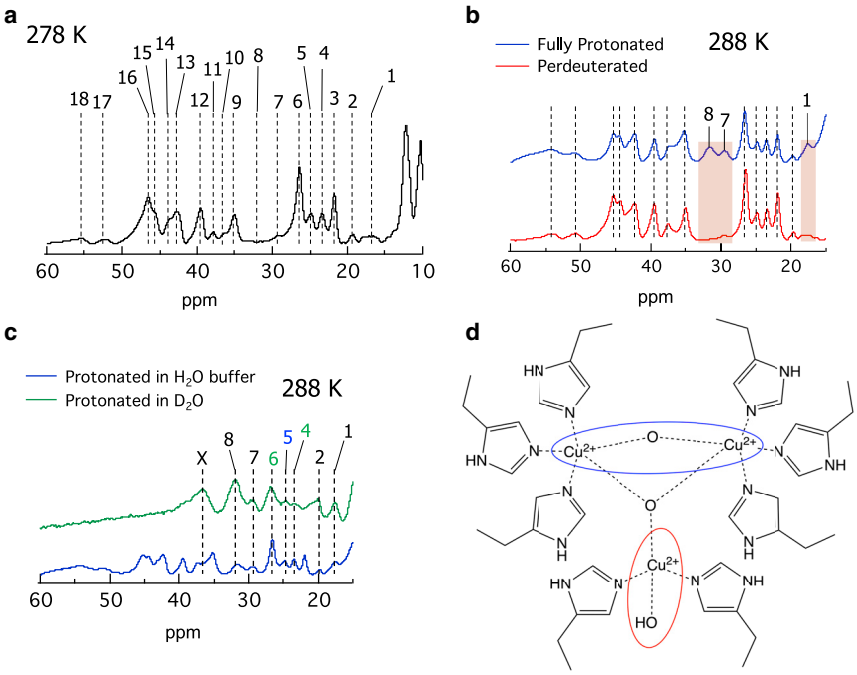

FIGURE 1 Analysis of the 1D ^{1}H spectra. (*a*) weft NMR spectra of a perdeuterated protein with amide proton back exchanged at 278 K depicting the part of the spectrum showing signals that are strongly shifted by Fermi contact effects; (*b*) 1D weft spectra at 288 K comparing samples that were fully protonated (*blue*) or perdeuterated with back exchange (*red*) both in H_2O buffer. The highlighted areas indicate the positions of resonances 1, 7, and 8, derived from protons attached to carbons; (*c*) 1D weft spectra at 288 K comparing fully protonated samples in D_2O buffer (*green*) and H_2O buffer (*blue*), showing the extensive loss of resonances because of the exchange of protons by deuterons. (*d*) Schematic representation of a TNC of small laccase in the NI state. The T3 and T2 sites are marked by blue and red ovals. Hδ1 His ring protons are shown.

enzyme is in the RO state (Scheme S1), whereas the SLAC-T1D form is in the NI state when isolated (Fig. 1 *d*; (17)). The theoretical molecular weight (MW) of the holoenzyme in its monomeric form is 37.05 kDa. The purified protein was found to run at an apparent MW of 75 and 37 kDa in sodium dodecyl sulfate polyacrylamide gel electrophoresis, but in solution, it has an MW ~105 kDa, as determined by size exclusion chromatography linked with multiangle light scattering. Thus, it is concluded that the enzyme is in its trimer form, as observed in crystal structure (18). The one-dimensional (1D) ^{1}H water-eliminated Fourier transform (weft) NMR (19) experiment enhances signals of protons experiencing rapid paramagnetic relaxation. The resulting spectrum of SLAC-T1D (Fig. 1 *a*) shows large Fermi contact shifts (FCS) for many resonances. The spectrum is very similar to the one reported by Machczynski et al. (6,17), confirming that TNC is fully formed. Fermi contact interactions fall off rapidly with the number of bonds between the metal and nucleus (20), indicating that the resonances with large shifts must derive from side chains of the copper-coordinating amino acid residues, which are histidines (21,22). Because the anisotropy of the copper sites in proteins is reported to be low (20), the contribution of pseudocontact shifts to the observed chemical shift is much smaller than that of the FCS, though not necessarily negligible in all cases (maximal pseudocontact shift estimations are provided in Table S7 using Eq. S14).

Temperature dependence of the FCS resonances (Fig. S10 *a*) showed three types of behavior: strong Curie (decreasing hyperfine coupling with increasing temperature) for resonances 11, 13, 16, 15, 18, and 17; weak anti-Curie (increasing hyperfine coupling with increasing temperature) for resonances 3, 6, 7, and 8; and no Curie (temperature independent) for resonances 4, 5, 9, and 12, suggesting that there is more than one coupled copper pair, in line with previous reports (17,23). The Supporting Materials and Methods presents an analysis of the quantitative analysis of the coupling scheme (Fig. S10 and Supporting Materials and Methods, Section S5).

Utilizing different deuteration schemes, resonances from protons attached to nitrogen and oxygen atoms can be distinguished from those attached to carbon, being exchangeable and nonexchangeable, respectively. For a per-deuterated sample that was allowed to back exchange the exchangeable deuterons to protons, resonances 1, 7, and 8 were lost from the spectrum, indicating that they derive from nonexchangeable, carbon-attached protons. The remaining resonances appear in the spectrum of this sample, indicating that they are from exchangeable protons, most likely attached to nitrogen atoms (Fig. 1 *b*). A normal, protonated sample in which exchangeable protons were replaced with deuterons by bringing the sample in D_2O yields a spectrum in which resonances 1, 7, and 8 are prominent, supporting the observation that the equivalent protons are attached to carbons (Fig. 1 *c*). For resonances 2, 4, 5, and 6 (Fig. 1 *a*), the assignment is less clear; they may represent overlapping signals from exchangeable and nonexchangeable protons (Fig. 1, *b* and *c*). The resonance marked X is from the broad signal that is present below resonances 9 and 10 in the fully protonated sample in H_2O buffer.

To probe the dynamics at the TNC, ^{1}H-^{1}H exchange spectroscopy (EXSY) (24) was used with solvent presaturation

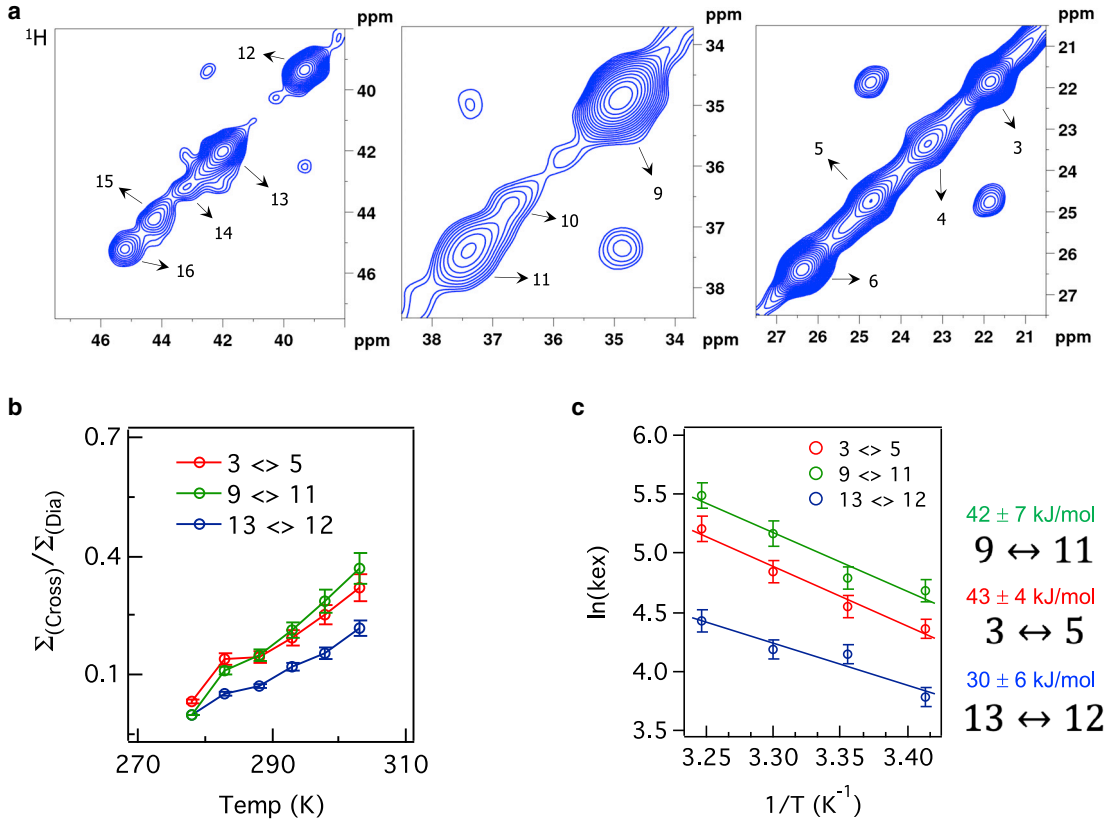

Figure360▷ **FIGURE 2 For a Figure360 author presentation of this figure, see https://doi.org/10.1016/j.bpj.2020.05.022 Exchange effects. (*a*) 2D ^{1}H-^{1}H EXSY spectra of the region between 21 and 47 ppm, showing resonances with exchange crosspeaks. The spectrum was recorded at 288 K at 14.2 T (600 MHz). The numbering of the resonances is equivalent to that of Fig. 1 *a*. (*b*) Temperature dependence of the sum of crosspeak intensity, normalized with the sum of the diagonal peak intensity of the resonances 3–5, 9–11, and 13–12 in red, green, and blue, respectively. The error bars are calculated from the noise level. (*c*) Arrhenius plot and the respective activation energies for the exchange processes 3 → 5, 9 → 11, and 13 → 12. The error is 1 SD.**

during the interscan delay and mixing time. We observe multiple crosspeaks between the FCS resonances (>10 ppm; Fig. S2). NOE (Nuclear Overhouser Effect) and exchange crosspeaks were distinguished by comparing the temperature dependence of the crosspeak intensities, which were normalized by the diagonal peak intensities. For the temperature range used in this work (278–303 K), NOE crosspeak intensity will be independent with respect to temperature, whereas the EXSY crosspeak intensity will show an increase with increasing temperature (Figs. 2, *a* and *b* and S2; (20)). The crosspeaks between resonances 3 and 5, 9 and 11, and 12 and 13 arise from chemical exchange, whereas the crosspeak between resonance 12 and a resonance at 11 ppm is an NOE crosspeak (Fig. S2). Resonances between 27 and 30 ppm belong to protons attached to carbon atoms. Crosspeaks were also observed between resonance pairs of 18–16 and 17–15 at very short mixing times of 1 and 2 ms and at 303 K (Fig. S4), but because of low signal-to-noise ratio, it could not be established whether these crosspeaks are due to chemical exchange or NOE. For resonances between 10 and 22.5 ppm, crosspeaks between six pairs of resonances were observed (Fig. S5, *a* and *b*). The temperature dependence of the crosspeak intensities normalized to the intensity at 293 K (Fig. S5 *c*) is somewhat irregular, showing a ~2-fold intensity increase between 293 and 308 K for peaks b and d, suggesting that they could be caused by chemical exchange. For the remaining crosspeaks (a, c, e, and f) it was not possible to classify them as either a chemical exchange or NOE derived because of the ambiguous temperature dependence or the low signal-to-noise ratio.

Thus, in the further analysis, we focused on the exchange peaks between resonances 3−5, 9−11, and 13−12. The chemical exchange is in the slow-exchange regime because a distinct resonance is observed for each state. The forward and backward chemical-exchange rates were determined for the three pairs of resonances using equations derived previously (Eq. S1; see also, Fig. S3; (25)). Table 1 summarizes the exchange rates obtained from fittings of the ratio of the cross by diagonal peak intensities at different temperatures. The equilibrium constant is ~0.5 and does not change much in the applied temperature range, but the exchange rates increase about twofold between 293 and 308 K for each resonance pair, allowing an estimation of the activation energy of the transition between the two states. The observed

TABLE 1 Kinetic Parameters and Equilibrium Constants

	3–5 (s^{-1})				9–11 (s^{-1})				13–12 (s^{-1})			
Temperature (K)	k_A	k_B	k_{ex}	K_{eq}	k_A	k_B	k_{ex}	K_{eq}	k_A	k_B	k_{ex}	K_{eq}
293	34	45	79	0.76	48	61	109	0.78	15	29	44	0.52
298	33	62	95	0.53	29	91	120	0.32	29	34	63	0.85
303	46	81	127	0.56	48	127	175	0.37	22	44	66	0.50
308	68	115	183	0.59	81	160	241	0.50	36	48	84	0.75

The values (error is estimated to be $\sim \pm 5\%$ from duplicate measurements) were obtained from the best fit (Fig. S2) of the crosspeak and diagonal intensities of the resonance pairs 3–5, 9–11, and 13–12 to Eq. S1. The rate constants k_A and k_B are the forward and reverse rates, and k_{ex} is the total exchange rate ($k_A + k_B$). K_{eq} is the equilibrium constant obtained from the ratio of the diagonal peak integral volume at $\tau_{mix} = 0$ ms and was constrained during fitting.

activation energies for the transitions of resonances 3–5, 9–11, and 13–12 are 43 ± 4, 42 ± 7, and 30 ± 6 kJ/mol, respectively.

The FCS for the two states differ by ~3 ppm, a relatively small change for an absolute FCS in the order of 20–35 ppm, indicating a small change in the unpaired electron-spin density on the proton. In combination, these observations agree with an assignment of the resonances to the protons linked to the $N^{\delta 1}$ atoms of the imidazole rings of histidines that coordinate the coppers in the T3 and T2 sites. Such protons are exchangeable with the solvent, but the exchange is slow enough for the resonance to be observed because all but one $N^{\delta 1}$ atom in the TNC are hydrogen bonded (Table S5). These hydrogens will experience large FCS, being very close to the copper ions. A rearrangement of the imidazole ring, such as a small rotation, can leave the coordination intact, yet cause a slight change in spin density and thus in the FCS. An inspection of the crystal structures of prokaryotic multicopper oxidases (3-domain monomeric laccases) yielded two examples (Protein Data Bank, PDB: 3zx1 and 2xu9) (26,27) in which imidazole ring motions at the T3 site were captured (Fig. S6). In 3zx1 (resolution 1.95 Å), two conformations of the His-182 ring are observed with $\chi 2$ angles 154 and 86°, yet maintaining a coordination bond with the T3-Cu (26). In structure 2xu9 (resolution 1.5 Å), the equivalent ligand, His-137, also displays two conformations, one of which has no coordination bond with T3-Cu. In this case, the $\chi 1$ angle also differs.

To estimate how much motion of the His rings could be accommodated at the TNC of SLAC, we modeled the change in distance between the T3-Cu and His $N^{\varepsilon 2}$ of the ligand His-158, equivalent to His-182.A in PDB: 3zx1, as a function of the $\chi 2$ dihedral angle, using PDB: 3cg8 (resolution 2.68 Å) (18). Allowing for a somewhat arbitrary maximal increase of 0.05 Å of the distance to maintain the coordination bond and avoiding clashes with surrounding atoms and maintaining the hydrogen bond of the $N^{\delta 1}$, the $\chi 2$ angle of His-158 can still assume values between 100 and 140° (Fig. S7). A similar analysis was done for all the coordinating His at the TNC (Fig. S8). In each case, the imidazole ring has considerable freedom to rotate. An analysis of $\chi 2$ angles for a variety of two-domain and three-domain laccase structures reflects this freedom (Fig. S8). This suggests that such ring motions might be responsible for the observed exchange behavior. The detailed method is given in the Supporting Materials and Methods.

The NMR observations show the presence of at least three chemical-exchange processes at the TNC, and we wondered whether one of them belongs to a ligand at the T2 site. If heterogeneity is present at the T2 site, distinct sites may show up in the electron paramagnetic resonance (EPR) spectrum for the frozen protein. The low-temperature EPR spectrum of SLAC-T1D yields a signal for the T2 site, whereas the coppers in the T3 site are antiferromagnetically coupled and thus EPR silent. The 9.5 GHz (X-band) spectrum at 40 K (Fig. 3) reveals the copper hyperfine structure in the low-field part of the spectrum, the g_z region from 265 to 320 mT, be it not a simple pattern of four equidistant lines. In addition to the copper hyperfine structure, the spectrum

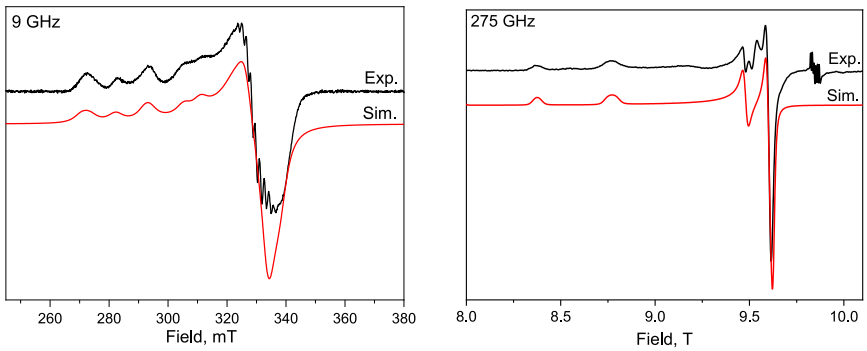

FIGURE 3 Experimental and simulated EPR spectra of the resting form of SLAC-T1D (as purified) at microwave frequencies of 9.5 and 275 GHz. The small signals around 9.85 T in the experimental spectrum at 275 GHz arise from an Mn (II) impurity in the sample. The hyperfine interaction of the copper electron spin with the nitrogen nuclei of the copper-coordinating histidines is not taken into account for the simulations. The experimental and simulation details are summarized in Supporting Materials and Methods.

shows a small but resolved hyperfine structure around 328 mT, which derives from the interaction of the copper electron spin with the nitrogen nuclear spins of the copper-coordinating histidines. To interpret the X-band spectrum, we make use of the 275 GHz EPR spectrum taken at 10 K (Fig. 3). At this high microwave frequency, the copper and nitrogen hyperfine structure is masked by line broadening due to the g-strain. The higher g-resolution at this frequency clearly reveals two distinct signals in the g_z region, at 8.37 and 8.77 T, corresponding to $g_z = 2.352$ and $g_z = 2.246$. Starting from these values, we simulated the EPR spectra at both microwave frequencies as the sum of the spectra of two components (Fig. 3), which differ in the g_y, g_z, and A_z spin Hamiltonian parameters (Table S6). The separate contributions of the two components to the simulated spectra are shown in Fig. S9. The parameters of the major component 1 correspond to those previously reported for the T2 site of SLAC-T1D (7), whereas the parameters of minor component 2 resemble those of the T2 site of multicopper oxidase from different organisms (Table S8 and references therein). The fraction of the minor component varies for different preparations and is commonly between 30 and 40%. We believe that the distinct EPR signals for SLAC-T1D are evidence of the heterogeneity in the T2 site of the TNC, in line with the observation of multiple states of the imidazole rings by NMR. The EPR spectrum at 275 GHz showing the difference in the value of g_z supports the presence of His ring motion at the T2 site because a rearrangement and rotation of an imidazole ring will affect the delocalization of electron density between copper and the imidazole, thereby changing the spin density on the copper that was determined through spin-orbit coupling to have the most sensitive g_z-value (28).

In conclusion, NMR spectroscopy showed that at least three independent chemical-exchange processes are present at the TNC, and EPR spectroscopy showed that heterogeneity exists at the T2 site. We propose that in the NI state of SLAC, there is a chemical exchange at the TNC, and this is due to the ring motions of coordinating histidine residues. The motions appear not to be concerted. Though the activation energies are similar within their error ranges, the exchange rates differ significantly (Table 1), indicating independent processes. Such motions could well be a general property of histidine rings, much like ring flips of aromatic residues. His ring flips in the influenza A M2 proton channel are associated with proton conduction, with an energy barrier greater than 59 kJ/mol (29). A fast His flip ($\sim$2000 s^{-1}) was described in detail for the surface-exposed, noncoordinating His-61 in plastocyanin from *Anabaena variabilis* (30). Here, the imidazole rings are not flipping (i.e., not rotating by 180°) because that would break the coordination bond, yet clearly two states exist, separated by a considerable activation barrier, perhaps representing two ring orientations with favorable coordination properties. It needs to be determined whether the same motions are present in wt SLAC. Given their local nature and the similarity in structures of T1D and wt laccases (17,18), it seems quite likely that such motions also occur in wt SLAC. Whether evolution has used His ring motions to the benefit of catalysis by SLAC, for example as a gatekeeper or for proton transfer, remains to be established.

SUPPORTING MATERIAL

Supporting Material can be found online at https://doi.org/10.1016/j.bpj.2020.05.022.

AUTHOR CONTRIBUTIONS

M.U. and H.J.M.d.G. conceived the project and acquired the funding. R.D. produced the protein and performed the NMR experiments. R.D. and M.U. analyzed the data. R.D. and K.B.S.S.G. optimized the NMR pulse sequence. F.N. performed the EPR experiments. F.N., G.W.C., and E.J.J.G. analyzed the EPR data. R.D. and M.U. wrote the manuscript.

ACKNOWLEDGMENTS

We thank Lionel Ndamba for the help with protein preparation for EPR experiments and ZoBio (Leiden, the Netherlands) for performing size exclusion chromatography linked with multiangle light scattering on the purified protein samples.

The study was supported by Netherlands Magnetic Resonance Research School (NWO-BOO 022.005.029) and The Netherlands Organization for Scientific Research, Department of Chemical Sciences.

REFERENCES

1. Mano, N., and A. de Poulpiquet. 2017. O2 reduction in enzymatic biofuel cells. *Chem. Rev.* 118:2392–2468.
2. Solomon, E. I., A. J. Augustine, and J. Yoon. 2008. O2 reduction to H2O by the multicopper oxidases. *Dalton Trans.* 2008:3921–3932.
3. Heppner, D. E., C. H. Kjaergaard, and E. I. Solomon. 2014. Mechanism of the reduction of the native intermediate in the multicopper oxidases: insights into rapid intramolecular electron transfer in turnover. *J. Am. Chem. Soc.* 136:17788–17801.
4. Lee, S.-K., S. D. George, …, E. I. Solomon. 2002. Nature of the intermediate formed in the reduction of O(2) to H(2)O at the trinuclear copper cluster active site in native laccase. *J. Am. Chem. Soc.* 124:6180–6193.
5. Palmer, A. E., S. K. Lee, and E. I. Solomon. 2001. Decay of the peroxide intermediate in laccase: reductive cleavage of the O-O bond. *J. Am. Chem. Soc.* 123:6591–6599.
6. Machczynski, M. C., E. Vijgenboom, …, G. W. Canters. 2004. Characterization of SLAC: a small laccase from Streptomyces coelicolor with unprecedented activity. *Protein Sci.* 13:2388–2397.
7. Tepper, A. W. J. W., S. Milikisyants, …, G. W. Canters. 2009. Identification of a radical intermediate in the enzymatic reduction of oxygen by a small laccase. *J. Am. Chem. Soc.* 131:11680–11682.
8. Gupta, A., I. Nederlof, …, G. W. Canters. 2012. Involvement of Tyr108 in the enzyme mechanism of the small laccase from *Streptomyces coelicolor*. *J. Am. Chem. Soc.* 134:18213–18216.
9. Wang, J., K. Wang, …, X.-H. Xia. 2014. Bioinspired copper catalyst effective for both reduction and evolution of oxygen. *Nat. Commun.* 5:5285.

10. van Dijk, B., J. P. Hofmann, and D. G. H. Hetterscheid. 2018. Pinpointing the active species of the Cu(DAT) catalyzed oxygen reduction reaction. *Phys. Chem. Chem. Phys.* 20:19625–19634.

11. Langerman, M., and D. G. H. Hetterscheid. 2019. Fast oxygen reduction catalyzed by a copper(II) tris(2-pyridylmethyl)amine complex through a stepwise mechanism. *Angew. Chem. Int.Engl.* 58:12974–12978.

12. Thorum, M. S., J. Yadav, and A. A. Gewirth. 2009. Oxygen reduction activity of a copper complex of 3,5-diamino-1,2,4-triazole supported on carbon black. *Angew. Chem. Int.Engl.* 48:165–167.

13. Brookes, J. C. 2017. Quantum effects in biology: golden rule in enzymes, olfaction, photosynthesis and magnetodetection. *Proc. Math. Phys. Eng. Sci.* 473:20160822.

14. Dorner, R., J. Goold, …, V. Vedral. 2012. Effects of quantum coherence in metalloprotein electron transfer. *Phys. Rev. E Stat. Nonlin. Soft Matter Phys.* 86:031922.

15. Fröhlich, H. 1968. Long-range coherence and energy storage in biological systems. *Int. J. Quantum Chem.* 2:641–649.

16. Lloyd, S. 2011. Quantum coherence in biological systems. *J. Phys. Conf. Ser.* 302:012037.

17. Machczynski, M. C., and J. T. Babicz, Jr. 2016. Correlating the structures and activities of the resting oxidized and native intermediate states of a small laccase by paramagnetic NMR. *J. Inorg. Biochem.* 159:62–69.

18. Skálová, T., J. Dohnálek, …, J. Hašek. 2009. The structure of the small laccase from Streptomyces coelicolor reveals a link between laccases and nitrite reductases. *J. Mol. Biol.* 385:1165–1178.

19. Bertini, I., C. Luchinat, …, R. Pierattelli. 2005. NMR spectroscopy of paramagnetic metalloproteins. *ChemBioChem.* 6:1536–1549.

20. Bertini, I., C. Luchinat, …, E. Ravera. 2017. NMR of Paramagnetic Molecules: Applications to Metallobiomolecules and Models, Second Edition. Elsevier, Amsterdam, the Netherlands.

21. Bertini, I., C. Luchinat, and G. Parigi. 2002. Magnetic susceptibility in paramagnetic NMR. *Prog. Nucl. Magn. Reson. Spectrosc.* 40:249–273.

22. Bertini, I., C. Luchinat, …, R. Pierattelli. 2008. Perspectives in paramagnetic NMR of metalloproteins. *Dalton Trans.* 0:3782–3790.

23. Zaballa, M.-E., L. Ziegler, …, A. J. Vila. 2010. NMR study of the exchange coupling in the trinuclear cluster of the multicopper oxidase Fet3p. *J. Am. Chem. Soc.* 132:11191–11196.

24. Jeener, J., B. H. Meier, …, R. R. Ernst. 1979. Investigation of exchange processes by two-dimensional NMR spectroscopy. *J. Chem. Phys.* 71:4546–4553.

25. Farrow, N. A., O. Zhang, …, L. E. Kay. 1994. A heteronuclear correlation experiment for simultaneous determination of ^{15}N longitudinal decay and chemical exchange rates of systems in slow equilibrium. *J. Biomol. NMR.* 4:727–734.

26. Silva, C. S., P. Durão, …, I. Bento. 2012. Crystal structure of the multicopper oxidase from the pathogenic bacterium Campylobacter jejuni CGUG11284: characterization of a metallo-oxidase. *Metallomics.* 4:37–47.

27. Serrano-Posada, H., S. Centeno-Leija, …, E. Rudiño-Piñera. 2015. X-ray-induced catalytic active-site reduction of a multicopper oxidase: structural insights into the proton-relay mechanism and O2-reduction states. *Acta Crystallogr. D Biol. Crystallogr.* 71:2396–2411.

28. van Gastel, M., J. W. A. Coremans, …, E. J. J. Groenen. 2002. An ab initio quantum-chemical study of the blue-copper site of azurin. *J. Am. Chem. Soc.* 124:2035–2041.

29. Hu, F., W. Luo, and M. Hong. 2010. Mechanisms of proton conduction and gating in influenza M2 proton channels from solid-state NMR. *Science.* 330:505–508.

30. Hass, M. A. S., D. F. Hansen, …, L. E. Kay. 2008. Characterization of conformational exchange of a histidine side chain: protonation, rotamerization, and tautomerization of His61 in plastocyanin from *Anabaena variabilis*. *J. Am. Chem. Soc.* 130:8460–8470.